Eur. Phys. J. E **15**, 311–318 (2004)
DOI 10.1140/epje/i2004-10071-7

THE EUROPEAN PHYSICAL JOURNAL E

Numerical analysis of the Eckhaus instability in travelling-wave convection in binary mixtures

I. Mercader[a], A. Alonso, and O. Batiste

Departament de Física Aplicada, Universitat Politècnica de Catalunya, Campus Nord, Mòdul B4, 08034 Barcelona, Spain

Received 22 July 2004 and Received in final form 10 October 2004 /
Published online: 22 November 2004 –

Abstract. The Eckhaus stability boundaries of travelling periodic roll patterns arising in binary fluid convection is analysed using high-resolution numerical methods. We present results corresponding to three different values of the separation ratio used in experiments. Our results show that the subcritical branches of travelling waves bifurcating at the onset of convection suffer sideband instabilities that are restabilised further away in the branch. If this restabilisation is produced after the turning point of the travelling-wave branch, these waves do not become stable in a saddle node bifurcation as would have been the case in a smaller domain. In the regions of instability of the uniform travelling waves we expect to find either transitions between states of different wave number or modulated travelling waves arising in these bifurcations.

PACS. 47.20.Ky Nonlinearity (including bifurcation theory) – 47.20.Bp Buoyancy-driven instability – 47.27.Te Convection and heat transfer – 47.54.+r Pattern selection; pattern formation

1 Introduction

The stability of a binary fluid layer subject to a vertical temperature gradient has been the subject of extensive experimental and theoretical research [1,2]. It is well known that the interplay of the different mechanisms involved in the system can lead to an oscillatory instability, which results in either travelling waves or standing waves in translation invariant systems. Experimentally, the realisation of translation invariant systems that can support uniform travelling waves has to be done with annular cells. Rectangular systems, however large they are, have the translation symmetry broken and the bifurcating solutions cannot be spatially uniform.

The oscillatory instability in binary fluid convection is usually subcritical, and convective motion begins in the form of growing oscillations. In annular systems, the pattern in these transient motions consists in the superposition of spatially modulated low-amplitude waves travelling in both directions (irregular standing waves), which grow until a final nonlinear state is selected. The final state depends strongly on the parameters of the mixture, especially on the separation ratio, and can take the form of large-amplitude travelling waves, steady convection rolls or highly irregular states in the form of confined travelling waves or spatiotemporal chaotic motions.

In order to clarify the origin of the different dynamical states, both careful experiments [3,4] and numerical simulations [5] have been performed in this system using water-ethanol mixtures as the convecting fluid.

In the extensive numerical work of Barten *et al.* [5], the branches of travelling waves (TW) and steady states (SOC) have been studied in detail for different values of the separation ratio. The system they consider is a two-dimensional cell such that only a single wavelength fits in the domain (the length of the cell is usually two times its height). In this way, the authors have obtained the bifurcation diagrams of the uniform TW and SOC states and have located the transition between them.

In periodic extended systems (large aspect ratio cells), solutions with slightly different wavelengths can fit into the domain, and we expect to find multistability and transitions between these states. In experiments in large annular containers, different behaviours have been observed depending on the separation ratio of the mixture. For instance, in the experiment reported in [3] for a value of the separation ratio of $S = -0.257$, when the threshold of stability of the conduction state is crossed, the final state consists of large-amplitude travelling waves. In this experiment, the travelling-wave branch is stable until a saddle node bifurcation is reached by decreasing the Rayleigh number. In contrast, in experiments with a separation ratio value closer to zero [4], $S = -0.021$, uniform travelling waves are never observed, despite numerical computations confirming their existence [5].

These completely different behaviours may be attributed to the different stability properties of the travelling-

[a] e-mail: isabel@fa.upc.edu

wave solutions when extended domains are considered, due to Eckhaus instabilities (instabilities that modify the periodicity of the basic solution).

The Eckhaus instability for travelling waves has been analysed in diverse convection problems, either experimentally, numerically or theoretically. One of the first studies was carried out in convection in a radially heated cylindrical annulus. The Eckhaus instability of the thermal Rossby waves was analysed by means of Direct Numerical Simulation of the full PDEs, in terms of a spatial Floquet parameter; both in the case of the small-gap approximation [6,7] or retaining the curvature [8]. In the context of the Rayleigh-Bénard convection, Janiaud *et al.* [9] have studied this instability experimentally in a short annular container for a low-Prandtl-number pure fluid. The analysis of the experimental results is based on a nonlinear phase equation that can be derived from a complex Ginzburg-Landau equation describing the slow dynamics near the onset of the oscillatory instability. The results seem to correspond to a subcritical Eckhaus instability. In thermosolutal convection [10], numerical simulations of the evolution equations in large periodic domains have shown the existence of transient long-wavelength modulations of the travelling waves, indicating the possible presence of an Eckhaus instability in this system.

At least two experimental papers have been devoted to the determination of the Eckhaus stability boundaries of travelling waves in binary fluid convection [11,12]. Other theoretical and numerical works have likewise considered the stability of extended patterns in binary fluid convection. Huke *et al.* [13] have analysed the stability of steady rolls and square convection for positive separation ratio mixtures, including in their analysis the Eckhaus instability. In [14] transitions between different wave number travelling-wave patterns have been observed in 2D numerical simulations considering finite containers for negative separation ratios, and the dynamics has been explained as a manifestation of Eckhaus instabilities.

The purpose of this paper is the actual determination of the sideband instabilities for travelling waves in binary fluid convection in periodic domains of aspect ratio around 80, corresponding to the experiments reported in [11,12], with the aim of explaining the different behaviours observed in experiments. The methodology has been to calculate the solution branches using a continuation strategy, and to perform a stability analysis of these states against wave patterns that either keep the spatial periodicity of the basic solution or break it.

The paper is organised as follows. In Section 2 the mathematical model is presented along with a description of the numerical methods used for the calculations. In Section 3 we present the results of our analysis, and finally the results and main conclusions are summarised in Section 4.

2 Mathematical model

We consider Boussinesq binary fluid convection in a narrow annular cell in the presence of a vertical gravity $\mathbf{g} = -g\hat{\mathbf{e}}_z$. A vertical temperature gradient is imposed by fixing a temperature difference ΔT between the horizontal plates, with the temperature at the bottom being higher than at the top. We are interested in modelling experiments in cells with cross-section width of the same order of the height d, and mean circumference L much larger than d [11,12]. It is well known that in such systems convection settles in the form of straight rolls with the axis in the radial direction, the dynamics being purely two dimensional. In accordance with this, we use a simplified geometry consisting of a two-dimensional domain $(x, z) \in [0, L] \times [0, d]$, with the aspect ratio Γ defined as $\Gamma = L/d$ much greater than one. This system admits the following basic conductive state with constant gradients of temperature and concentration:

$$\mathbf{u}_\mathrm{c} = 0, \tag{1a}$$

$$T_\mathrm{c} = T_0 - \Delta T\left(\frac{z}{d} - \frac{1}{2}\right), \tag{1b}$$

$$C_\mathrm{c} = C_0 + C_0(1 - C_0)S_T\Delta T\left(\frac{z}{d} - \frac{1}{2}\right), \tag{1c}$$

where $\mathbf{u} = (u, w)$ is the velocity field; T and C are the fields of temperature and concentration of the denser component, respectively; T_0 and C_0 are their mean values, and S_T is the Soret coefficient.

The dynamics of the system is governed by the continuity equation, the Navier-Stokes equations and the energy and mass conservation equations [15]. In their nondimensional form, by using the height of the layer d, d^2/κ and ΔT as scales for length, time and temperature, respectively, κ being the thermal diffusivity, the equations explicitly read

$$\boldsymbol{\nabla}\cdot\mathbf{u} = 0, \tag{2a}$$

$$\partial_t\mathbf{u} + (\mathbf{u}\cdot\boldsymbol{\nabla})\mathbf{u} = -\boldsymbol{\nabla}p + \sigma\nabla^2\mathbf{u} + R\sigma[(1+S)\Theta + S\eta]\hat{\mathbf{e}}_z, \tag{2b}$$

$$\partial_t\Theta + (\mathbf{u}\cdot\boldsymbol{\nabla})\Theta = w + \nabla^2\Theta, \tag{2c}$$

$$\partial_t\eta + (\mathbf{u}\cdot\boldsymbol{\nabla})\eta = -\nabla^2\Theta + \tau\nabla^2\eta. \tag{2d}$$

Here, Θ denotes the departure of the temperature from its conduction profile, $\Theta = (T - T_\mathrm{c})/\Delta T$, and $\eta = -(C - C_\mathrm{c})/(C_0(1 - C_0)S_T\Delta T) - \Theta$. The dimensionless parameters in the above equations are the Rayleigh number, R, the Prandtl number, σ, the Lewis number, τ, and the separation ratio, S, defined as

$$R = \frac{\alpha\Delta T g d^3}{\kappa\nu}, \quad \sigma = \frac{\nu}{\kappa}, \quad \tau = \frac{D}{\kappa}, \quad S = C_0(1 - C_0)\frac{\beta}{\alpha}S_T,$$

where α and β are the thermal and concentration expansion coefficients, ν is the kinematic viscosity and D is the mass diffusivity.

The boundary conditions are taken to be periodic in x with period Γ. No-slip, fixed temperature and no mass flux at the top and bottom plates are considered

$$\mathbf{u} = \Theta = \partial_z\eta = 0 \qquad \text{on} \quad z = 0, 1\,. \tag{3}$$

As a measure of the heat transport by convection, we use the Nusselt number Nu, defined as the ratio of heat

flux through the top plate to that of the corresponding conductive solution. It has the following expression:

$$Nu = 1 - \Gamma^{-1} \int_{x=0}^{x=\Gamma} \partial_z \Theta(z=1) \mathrm{d}x.$$

Equations and boundary conditions are equivariant under the two reflections,

$$R_0 : (x,z) \to (-x,z), \qquad (u,w,\Theta,\eta) \to (-u,w,\Theta,\eta),$$

$$R_z : (x,z) \to (x,1-z), \quad (u,w,\Theta,\eta) \to (u,-w,-\Theta,-\eta),$$

and under translations of a distance ℓ,

$$T_\ell : (x,z) \to (x+\ell,z), \qquad (u,w,\Theta,\eta) \to (u,w,\Theta,\eta).$$

The reflection R_0 is with respect to an arbitrarily chosen origin in x; reflections R_{ℓ_0} with respect to a plane $x = \ell_0$, say, are obtained by conjugation: $R_{\ell_0} = T_{\ell_0} R_0 T_{-\ell_0}$. These symmetries generate the symmetry group $\mathbf{O}(2) \times \mathbf{Z}_2$. The conduction state $\mathbf{u} = \Theta = \eta = 0$ is invariant under this group.

For sufficiently negative values of the separation ratio, which is the case considered here, the onset of instability is oscillatory and the translation invariance is broken, *i.e.* the wave number k of the dominant perturbation is nonzero, and a pattern of wavelength $a = 2\pi/k$ appears. As expected in this type of Hopf bifurcation with $\mathbf{O}(2)$ symmetry, two branches of nontrivial solutions bifurcate simultaneously [16]. The instability evolves either to a pattern of standing waves (SW) or into waves that travel in either x-direction (TW). For the parameters chosen in this paper, if we fix the wave number k and we use the Rayleigh number as a bifurcation parameter, the TW branch typically bifurcates subcritically (see Fig. 1), acquiring stability at a secondary saddle node bifurcation. When the Rayleigh number is increased from the saddle node point, the TW branch disappears in a parity-breaking bifurcation of steady solutions called SOC states (stationary overturning convection), to which stability is transferred [2]. The standing waves (SW) are unstable from the onset and usually disappear in a global bifurcation in which the SW connects with an unstable SOC state. The primary instability also breaks the midplane reflection symmetry R_z. However, since this instability is oscillatory, the bifurcating periodic solutions (TW and SW) possess a space-time symmetry such that the spatial action of R_z is exactly compensated by an evolution in time by half a period. For a TW or a SW, this also implies that these solutions are invariant under the mirror-glide symmetry $T_{a/2}R_z$ [5], *i.e.* the spatial action of R_z is exactly compensated by a translation in space by half a basic wavelength, $a/2$. As a summary, we can say that the SOC and the bifurcating SW states possess the same symmetries as the primary rolls in 2D thermal convection [17], *i.e.* R_{l_0} and $T_{a/2}R_z$, whereas TW states are only $T_{a/2}R_z$ invariant, which implies that they have a z-symmetric horizontal mean flow.

As far as the numerical method is concerned, we use spectral methods for the spatial discretisation: Fourier-Galerkin in x and Chebyshev collocation in z. Different codes have been used depending on the type of solutions we try to obtain.

Most of the calculations carried out in this paper are aimed at obtaining spatial periodic solutions (either SOC or TW states) that, fitting in the domain of periodicity Γ, contain many wavelengths a; this is the spatial periodicity we have imposed. To calculate these steady solutions we have adapted a first-order time-stepping formulation to carry out Newton's method, as described in [18,19]. In the preconditioned version of Newton's iteration, the corresponding linear system is solved by an iterative technique using a GMRES package [20]. Travelling waves have been obtained in a similar way, by assuming time-independent functions $g_n(z)$ in the following Fourier expansion of any variable:

$$\chi_{\mathrm{TW}}(x,z,t) = \sum_{n=-N}^{N} g_n(z) e^{ink(x-ct)}, \tag{4}$$

being $k = \frac{2\pi}{a}$ the basic wave number. Letting $\tilde{x} = x - ct$, we solve a steady problem. By adding an equation to fix the phase of the solution, the phase velocity c can be determined. Steady and travelling waves have also been calculated with a Newton-Raphson iterative scheme in a streamfunction formulation [21,22,8].

To study the stability of two-dimensional waves in a periodic box that contains M basic wavelengths a, we proceed in the same way as in [21]. Since the basic solution has period a, the associated linear operator has the same periodicity and, according to Floquet theory, the set of perturbations splits as

$$\{\chi_m^*(\tilde{x},z,t) = \chi_m(\tilde{x},z) e^{id_m k\tilde{x}} e^{\lambda_m t}\}_{m=0\ldots M-1}, \tag{5}$$

where

$$\chi_m(\tilde{x},z) = \chi_m(\tilde{x}+a,z) \tag{6}$$

with $d_m = m/M$ being the spatial Floquet parameter. Thus $\chi_m^*(\tilde{x},z,t)$ admits the following development:

$$\chi_m^*(\tilde{x},z,t) = \sum_{n=-N}^{N} g_n^*(z) e^{i(n+d_m)k\tilde{x}} e^{\lambda_m t}. \tag{7}$$

The corresponding eigenvalue problem has to be solved for every value of m. If for some value of m, the real part of λ_m is positive, the TW is unstable, otherwise it is stable. If $d = 0$, the perturbation has the same wavelength as the two-dimensional waves and the solution that bifurcates still contains M basic wavelengths. In this stability analysis, we always obtain a zero eigenvalue corresponding to the trivial phase-shift solution.

In the case $d \neq 0$, subharmonic disturbances are considered. The basic periodicity a is now broken and a new solution with a larger basic period emerges. As discussed in [22], the eigenfunctions for the problem with d_{M-m}, as well as the eigenvalues λ_{M-m}, can be obtained by conjugating those with d_m. Then it suffices to consider perturbations with $d_m \in (0, 1/2]$. Notice that if a train of uniform travelling waves of basic wave number k and frequency $\omega = ck$ suffers a bifurcation of this type

($\Re(\lambda) = 0$), additional wave numbers $k_n = (n + d_m)k$ and $k'_n = (n + d_{M-m})k$ are excited at first order in the bifurcating solution; the corresponding frequencies being $\omega_n = -(n + d_m)\omega + \omega^*$ and $\omega'_n = -(n + d_{M-m})\omega - \omega^*$, where $\omega^* = \Im(\lambda_m)$. Then, for the bifurcated solution near every pair of frequencies and wave numbers ($\omega_{0n} = n\omega, k_{0n} = nk$) of the basic solution, two pairs (ω_n, k_n) and $(\omega'_{n-1}, k'_{n-1})$ appear, which allows us to estimate the group velocity as

$$c_g \approx c + \frac{\omega^*}{d_m k}. \tag{8}$$

The linear stability analysis of the steady solutions (SOC) is carried out in a similar way, and the details can be found in reference [22].

To validate the stability analysis, time-dependent calculations considering the real periodicity Γ, have also been carried out. To do this, we use the second-order time-splitting algorithm proposed in reference [23], which has been successfully used in previous studies of binary mixtures in large aspect ratio containers [24].

3 Results

In this section we present the results obtained for binary mixtures with three different values of the separation ratio: $S = -0.021$, $S = -0.127$ and $S = -0.257$, corresponding to the water-ethanol mixtures used in the experiments of references [4,11,3]. The values of the Prandtl and Lewis number chosen are also those of the experiments, so they are slightly different in each case. In the first mixture we consider $\sigma = 6.22$ and $\tau = 0.009$, in the second one $\sigma = 6.86$ and $\tau = 0.0083$ and in the last $\sigma = 9.16$ and $\tau = 0.008$.

In Section 3.1 we discuss the dynamics of uniform states with basic wave number $k = \pi$, and we analyse the stability of the travelling-wave branch with respect to both subharmonic disturbances and perturbations that maintain the basic wave number. In Section 3.2 the previous stability analysis is extended to waves with basic wave number different from π. To analyse the Eckhaus instability, the aspect ratio of the container is taken to be $\Gamma = 80$ in the case of $S = -0.021$ and $S = -0.257$, and $\Gamma = 84$ in the $S = -0.127$ mixture.

Although the critical wave number in the two-dimensional case when the length of the container is considered to be infinity is slightly different from $k = \pi$, the critical wave number of the basic pattern in the problems we analyse ($\Gamma = 80$ and $\Gamma = 84$) is certainly $k = \pi$. Nevertheless, the selected wave number in the experiments may differ from $k = \pi$. On one hand, the number of pairs of rolls must be adapted to the actual length of the container. On the other, the width of the cell, which is neglected in the 2D computations, is known to affect the critical wave number of the pattern, as the linear stability analysis in finite-width containers proves [25].

3.1 Eckhaus instability in the branch of travelling waves with basic wave number k = π

Figure 1 shows the bifurcation diagrams for the three values of the separation ratio we are considering when the basic periodicity of the pattern is not allowed to vary. The Nusselt number has been plotted as a function of the Rayleigh number (the control parameter of the system). The diagrams include the branches of uniform travelling waves (TW) and steady-state (SOC) solutions with basic wave number π, which is the critical wave number in the cells considered and corresponds to rolls of wavelength 2. As usual, dashed and solid lines denote unstable and stable solutions, respectively. The precise location of the bifurcations presented in the three diagrams is indicated in Table 1. R_c denotes the critical Rayleigh number at the onset of convection, R_{SN}^{TW} the Rayleigh number at which the secondary stabilising saddle node bifurcation in the TW branch takes place, R^* the Rayleigh number of the parity-breaking bifurcation in which the TW branch disappears and transfers stability to the SOC solution and R_{SN}^{SOC} the Rayleigh number of the saddle node bifurcation in the SOC branch.

Each bifurcation diagram also includes the contour plots of the concentration field of a TW and a SOC solution computed in the upper part of the TW and SOC branches of solutions. For both types of solutions, the concentration field is nearly uniform within each roll and presents boundary layers between rolls, but concentration is different in adjacent rolls in a TW solution while it is the same in the stationary solution. By observing the contour plots, we see that the concentration plumes become narrower and steeper as the Rayleigh number increases. It is important to bear in mind that these layers need to be correctly resolved by the numerical method, so a high spatial resolution is required to compute strongly nonlinear solutions. The structure of the TW and SOC states has been discussed extensively in the work of Lücke *et al.* (*i.e.*, [2]).

Several differences in the bifurcation diagrams are observed as the value of the separation ratio becomes more negative. As is well known, the Soret effect stabilises the layer in negative separation ratio mixtures, so the onset of convection is delayed as $|S|$ increases in magnitude. Furthermore, the region of subcriticality, which is quite small for $S = -0.021$, becomes progressively more important with increasing $|S|$. As a result, the saturated nonlinear solution at the onset of convection is of larger amplitude in the case of $S = -0.257$. An indication of the amplitude of convection is given by the Nusselt number, which for the nonlinear stable state at the onset of convection, is in the case of $S = -0.257$ an order of magnitude larger than in the $S = -0.021$ case, as can be observed in the plots. The value of the separation ratio of the mixture also influences the position of the transition from travelling wave to SOC convection. As the value of $|S|$ increases, this bifurcation moves away from the saddle node bifurcation in the TW branch and occurs for a larger value of the Rayleigh number, so the region of existence of the travelling waves gets wider. Indeed, for such a small value of the separation ratio as $S = -0.021$, the stable nonlinear solution at the

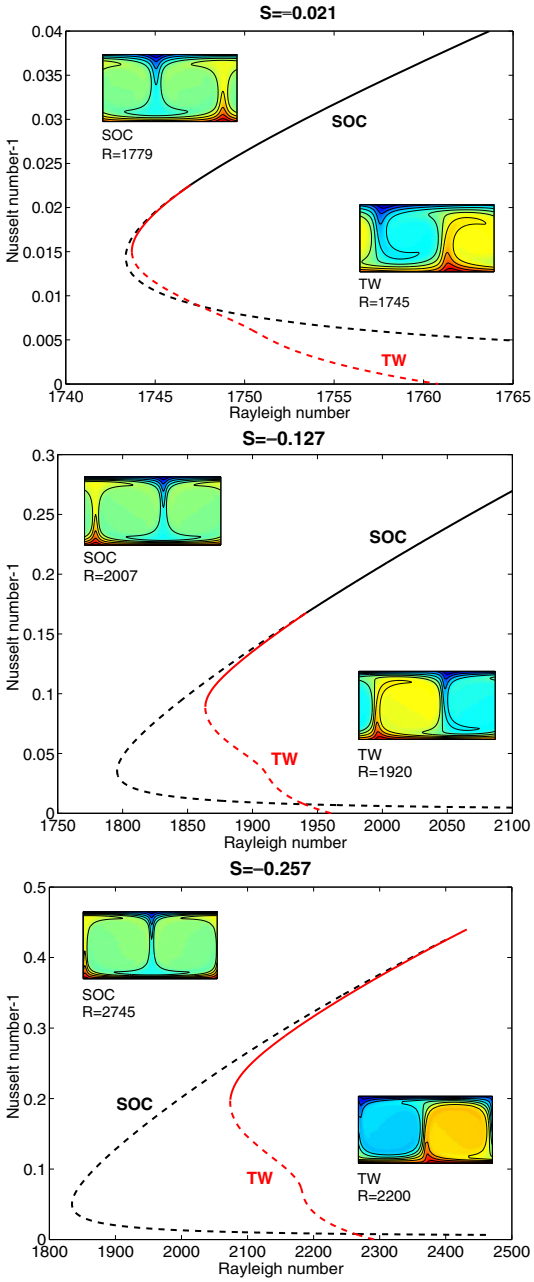

Fig. 1. Bifurcation diagrams (Nusselt number-1 *versus* the Rayleigh number) showing the SOC and TW branches of solutions of the wave number $k = \pi$ for three different sets of parameters corresponding to the experiments of references [4, 11,3]. From top to bottom: $(S = -0.021, \sigma = 6.22, \tau = 0.009)$, $(S = -0.127, \sigma = 6.86, \tau = 0.0083)$ and $(S = -0.257, \sigma = 9.16, \tau = 0.008)$. Each diagram includes a contour plot of the concentration field of a nonlinear TW and a SOC solution computed in the upper part of the TW and SOC branches.

onset is a SOC state, whereas for $S = -0.257$ nonlinear travelling waves are stable at the Rayleigh number of the onset of convection.

In order to find out how these bifurcation diagrams are modified when the periodicity of the basic solution is allowed to change, we have computed the Eckhaus instability in the TW branch, both in the lower part of the branch, before the saddle node bifurcation point, where travelling waves are unstable, and in the upper part, after the saddle node point. To analyse the stability of the travelling-wave solution with respect to subharmonic disturbances, the length of the box needs to be fixed. In the cases of $S = -0.021$ and $S = -0.257$, the aspect ratio of the cell we have considered is $\Gamma = 80$, which means that the basic solution of wave number $k = \pi$ corresponds to an $n = 40$ Fourier mode (*i.e.* the solution is formed by 40 pairs of rolls). In the case of $S = -0.127$, the choice for the length of the container is $\Gamma = 84$, therefore the basic solution of wave number $k = \pi$ now corresponds to an $n = 42$ Fourier mode.

Table 1. Critical values of the Rayleigh number of the bifurcations included in Figure 1 for the three cases considered there, $S = -0.021, -0.127, -0.257$. R_c indicates the primary Hopf bifurcation of the conductive state, R_{SN}^{TW} and R_{SN}^{SOC} the saddle node bifurcations in the branches of TW and SOC solutions and R^* the parity-breaking bifurcation of the SOC solutions, where the TW branch disappears.

S	R_c	R_{SN}^{TW}	R_{SN}^{SOC}	R^*
-0.021	1760.81	1743.69	1743.35	1746.96
-0.127	1960.5	1863.7	1795.8	1941.5
-0.257	2291.4	2073.7	1834.3	2431

For the binary mixture with $S = -0.257$, the computations show that, although several subharmonic bifurcations in the lower part of the TW branch have been identified, the stability of the $k = \pi$ TW branch is not modified when the Eckhaus instability is taken into account. The first destabilising Eckhaus bifurcation in the TW branch has Floquet parameter $d_1 = 1/40$ and takes place at $R = 2272$ (convection sets in at $R_c = 2291$). Successive destabilisations against perturbations of different Floquet parameters occur, but the TW solution regains stability against all these perturbations before the saddle node point is reached. Therefore, travelling waves with wave number $k = \pi$ go on acquiring the stability in the saddle node point. No Eckhaus bifurcations have been identified in the upper part of the TW branch, so the travelling waves remain stable until their connection with the SOC branch. The behaviour is very similar for the binary mixture with $S = -0.127$. Some destabilising bifurcations followed by the corresponding stabilising bifurcations take place in the $k = \pi$ TW branch. In this case, though, the last stabilising Eckhaus bifurcation is produced for a Rayleigh number $R = 1864.26$, which is slightly superior to that of the saddle node, $R_{SN}^{TW} = 1863.66$.

A different behaviour is obtained in the $S = -0.021$ mixture. The Eckhaus bifurcations that have been identified are included in Figure 2. The open circles show the location of the destabilising bifurcations, while the solid circles correspond to the stabilising ones. The first Eckhaus instability, with Floquet parameter $d_1 = 1/40$, occurs extremely soon, at $R = 1760.67$, which is nearly at the critical point ($R_c = 1760.81$). There are two more destabilising

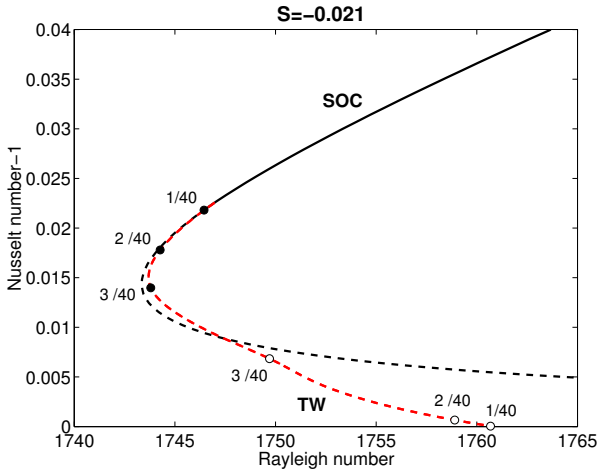

Fig. 2. Bifurcation diagram (Nusselt-1 *versus* the Rayleigh number) for a uniform train of travelling waves of wave number $k = \pi$ contained in a periodic domain of aspect ratio $\Gamma = 80$. The remaining parameters are $S = -0.021, \sigma = 6.22, \tau = 0.009$ (the parameters considered in the diagram at the top of Fig. 1). The points where subharmonic instabilities take place are indicated in the figure together with the corresponding Floquet parameter $d_{m/M}$. Following the curve of TW waves from the onset of convection, open and solid circles are used to indicate loss and gain of stability, respectively.

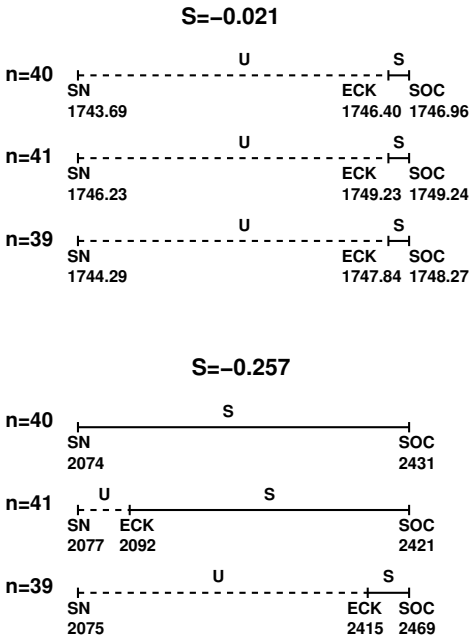

Fig. 3. Sketch of the stability regions of uniform TW solutions of different wave numbers contained in domains of aspect ratio $\Gamma = 80$ for the parameters: $S = -0.021$, $\sigma = 6.22$, $\tau = 0.009$, (top) and $S = -0.257$, $\sigma = 9.16$, $\tau = 0.008$ (bottom). We use n to indicate the number of pairs of rolls that fit in the periodic domain. Dashed and continuous lines denote unstable (U) and stable (S) regions. The values of the Rayleigh number of the boundaries of these regions are also given; SN is used for the saddle node of the TW branch; ECK is the point where the TW branch becomes Eckhaus stable, and SOC is the point where the TW branch finishes in a parity breaking of the SOC state.

bifurcations with Floquet parameters $d_2 = 2/40$ and $d_3 = 3/40$. In this case, the Eckhaus stability is not retrieved before the saddle node point. As can be clearly seen in the figure, the $k = \pi$ TW is Eckhaus unstable against disturbances of Floquet parameter d_1 until $R = 1746.40$, which is practically the position of the transition from TW to SOC ($R^* = 1746.96$). So in this case, the region of stability of the uniform travelling wave is extremely small. This result agrees with the experimental observations reported in [4], where nonlinear saturated TW states have not been observed.

3.2 Eckhaus instability for travelling waves with different values of the basic wave number

In large aspect ratio containers, stable uniform travelling waves with a slightly different value of the wave number can coexist with the critical solution. These solutions, which represent travelling waves with a different number of roll pairs ($n = \ldots 38, 39, 41, 42 \ldots$ in a box of length $\Gamma = 80$; $n = \ldots 40, 41, 43, 44 \ldots$ in a box of length $\Gamma = 84$), bifurcate from the conduction state for a value of the Rayleigh number very close to the critical one. Therefore, it is of interest to calculate these travelling waves and analyse their stability with respect to subharmonic disturbances, as is done in the previous section with the $k = \pi$ TW.

The results obtained for the mixtures with $S = -0.021$ and $S = -0.257$ in a box of aspect ratio $\Gamma = 80$ are summarised in a schematic way in Figure 3. The critical solution corresponds to the $n = 40$ TW, and only the adjacent solutions, $n = 39$ and $n = 41$ TW, have been plotted. Each straight line represents the upper part of the TW branch (after the saddle node bifurcating point). For each solution, the location of the saddle node point, of the last stabilising Eckhaus bifurcation and of the TW-SOC transition is indicated. The solid lines point out the regions of stability of the solution, while the dashed lines indicate that the corresponding uniform TW is Eckhaus unstable. As can be inferred from the figure, the behaviour is different depending on the value of the separation ratio. For $S = -0.021$, the $n = 39$ and $n = 41$ travelling waves behave like the $n = 40$ TW. They are Eckhaus unstable in most of the region between the saddle node and the TW-SOC transition; indeed they are only stable in a tiny interval of Rayleigh numbers. In contrast, for $S = -0.257$ the stability of the uniform TW depends very much on whether the number of rolls is increased or decreased with respect to the critical number of rolls. The critical $n = 40$ TW is stable in all the region. If there is an increase of one roll pair, $n = 41$ TW, the last Eckhaus bifurcation that stabilises the TW takes place at a Rayleigh number slightly superior to the one corresponding to the saddle node point, but the solution goes on being Eckhaus stable in a significant region. When there is a decrease in one roll

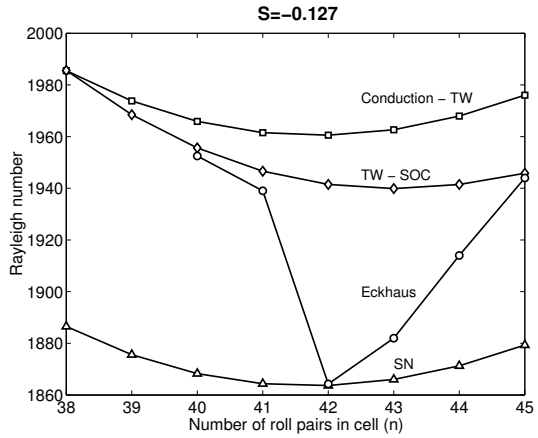

Fig. 4. Stability boundaries in a wave number (n)-Rayleigh number diagram corresponding to solutions for the parameters $S = -0.127, \sigma = 6.86, \tau = 0.0083, \Gamma = 84$ [11]. The bifurcation points for travelling waves containing a different number n of pair rolls are indicated by using: squares for the bifurcation of the conductive state, triangles for the saddle node bifurcation of TW solutions, diamonds for the parity-breaking bifurcation TW-SOC and circles for the Eckhaus instability which stabilises the TW branch.

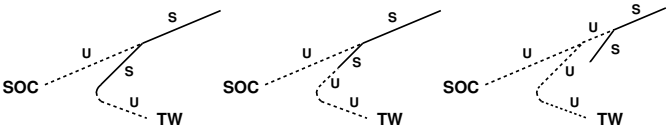

Fig. 5. Sketch of the different scenarios of stability diagrams containing SOC and TW solutions that we have found when these uniform states are contained in big periodic domains. On the left, the solution has become stable to every Floquet parameter at the lower branch before reaching the saddle node point, so the TW branch is stable from this point. In the middle, the solution becomes Eckhaus stable in the zone from the saddle node to the TW-SOC bifurcation, so the stability region of travelling waves is reduced. On the right, the branch TW solutions is unstable, and the SOC state gains stability further away from the TW-SOC bifurcation.

pair, $n = 39$ TW, the last Eckhaus bifurcation is shifted upward in the branch. As a result, the $n = 39$ TW is stable in a considerably smaller region than the $n = 40$ and $n = 41$ TW. This result seems to indicate that there is a trend to favour the stability of solutions with a wave number larger than the critical one (solutions with a larger number of pairs of rolls). This trend is also observed for the $S = -0.127$ mixture, as we will see below.

Finally, the results obtained from the analysis of the binary mixture with an intermediate value of the separation ratio, $S = -0.127$, in a box of $\Gamma = 84$ are included in Figure 4. In this figure we plot the Rayleigh number at the onset of convection (squares), the Rayleigh number at which the TW-SOC transition takes place (diamonds), the position of the last stabilising Eckhaus bifurcation (circles) and the saddle node point in the TW branch (triangles) as a function of the number of roll pairs in the cell. This defines the four corresponding stability curves. In this cell, the critical mode is the $n = 42$ TW, and it is Eckhaus stable from just above the saddle node point to the TW-SOC bifurcation. Travelling-wave solutions with $n = 40$, $n = 41$, $n = 43$ and $n = 44$ are stable only in a part of the region between the saddle node point and the TW-SOC transition. Again, the region of stability of the $n = 41$ TW is drastically reduced with respect to the $n = 42$ TW, while such a reduction does not take place for the $n = 43$ TW. Other travelling-wave solutions, such as the $n = 38$, $n = 39$ or $n = 46$ TW, are always unstable. As a consequence, the SOC solution is also unstable after the TW-SOC bifurcation. The Eckhaus bifurcation that stabilises the solutions with these wave numbers now takes place in the SOC branch. It is worth mentioning that, according to our results, the subharmonic bifurcation that stabilises the TW or the SOC solutions is always that with Floquet parameter $d_1 = 1/n$, irrespective of the number of rolls of the TW.

4 Discussion

In this paper we present the results for the travelling-wave Eckhaus instability in binary mixtures with different values of the separation ratio. Depending on the number of rolls of the uniform travelling wave and on the value of the separation ratio, the three different scenarios depicted in Figure 5 are possible. First, the uniform travelling wave can be stable against Eckhaus disturbances in the whole region between the saddle node bifurcating point and the TW-SOC transition (left diagram in Fig. 5). We have only obtained this behaviour in the case of the $n = 40$ TW in a box of length $\Gamma = 80$ for $S = -0.257$ (the $n = 42$ TW in a box of length $\Gamma = 84$ for $S = -0.127$ becomes stable slightly above the saddle node). Second, the uniform travelling wave can acquire the stability for a value of the Rayleigh number between the saddle node point and the TW-SOC bifurcation (middle diagram in Fig. 5). In principle, as expected, the region of stability of the uniform travelling wave becomes smaller as the difference in the number of roll pairs with the critical solution increases, but a tendency to favour the stability of solutions with a larger number of rolls compared with those with a smaller number has been identified for $S = -0.257$ and $S = -0.127$ mixtures. Finally, some uniform travelling waves are always Eckhaus unstable. In such cases, the SOC solution is still unstable after the TW-SOC bifurcating point, and acquires stability in a bifurcation that occurs for a larger value of the Rayleigh number (right diagram in Fig. 5).

It must be mentioned that the type of bifurcation is not the same when the last stabilising Eckhaus bifurcation takes place in the TW branch (first and second possibilities) as when it occurs in the SOC branch (third scenario). In the former case, the Eckhaus bifurcation is a Hopf bifurcation, and modulated travelling waves (both in time

and in space) will arise. If this bifurcation is supercritical, the modulated travelling waves will be observed, as happens in the two-dimensional Poiseuille flow [21]. The pulses leading to the appearance of spatially nonuniform wave trains described in [10] for thermosolutal convection also exhibit a behaviour that would be typical of such modulated travelling waves. However, if the bifurcation is subcritical, transients that bring the uniform solution back within the stable band, involving a change in the number of rolls such as those observed in experiment [12], are expected to occur. In the latter case, the Eckhaus bifurcation is found to be stationary. Nevertheless, the arising pattern might also travel slowly as a result of the parity breaking produced in the bifurcation point. The slowly travelling patterns reported in the experiment [3], which coexist with the SOC solution might arise from an Eckhaus instability in a SOC branch. However, these patterns could also result from a breakdown of the pitchfork bifurcation from SOC to TW due to the presence of spatial inhomogeneities in the system, as argued in [26].

The stability properties of the uniform TW solution obtained with the Eckhaus analysis have been confirmed with some computations performed with the time-evolution code.

Our stability analyses for the $S = -0.021$ mixture are in total agreement with the observations in the experiment [4]. In this experiment no stable nonlinear travelling waves are observed irrespective of the value of the Rayleigh number. Our Eckhaus stability analysis determines that all the uniform travelling waves we have analyzed are indeed Eckhaus unstable until the TW-SOC bifurcation point is nearly reached. On the other hand, the comparison between our results for the $S = -0.127$ binary mixture and the experimental observations reported in [11] show some discrepancies. First, the minimum of the experimental Eckhaus curve is not obtained for an $n = 42$ TW (which is the minimum of the curve for the onset of convection) but for $n = 40$. Apart from this, the Eckhaus stability boundary, which is not symmetric as in our results, seems to present just the opposite trend: the region of Eckhaus stability of the travelling waves with a smaller number of roll pairs is larger than that of the waves with a larger number of rolls. We believe that the cause of these discrepancies might be the finite width of the experimental cell, which is neglected in our computations.

We are particularly grateful to M. Lücke for helpful discussions. This research has been funded by DGICYT grant BFM2003-00657.

References

1. M.C. Cross, P.C. Hohenberg, Rev. Mod. Phys. **65**, 998 (1993).
2. M. Lücke, W. Barten, P. Büchel, C. Fütterer, St. Hollinger, Ch. Jung, *Evolution of Spontaneous Structures in Dissipative Continuous Systems*, edited by F.H. Busse, S.C. Müller (Springer-Verlag, Berlin, Heidelberg, 1998) pp. 127-196.
3. D.R. Ohlsen, S.Y. Yamamoto, C.M. Surko, P. Kolodner, Phys. Rev. Lett. **65**, 1431 (1990).
4. P. Kolodner, J.A. Glazier, H. Williams Phys. Rev. Lett. **65**, 1579 (1990).
5. W. Barten, M. Lücke, M. Kamps, R. Schmitz, Phys. Rev. E **51**, 5636 (1995).
6. A.C. Or, F.H. Busse, J. Fluid Mech. **174**, 313 (1987).
7. A.C. Or, F.H. Busse, J. Fluid Mech. **245**, 155 (1992).
8. D. Pino, M. Net, J. Sánchez, I. Mercader, Phys. Rev. E **63**, 056312 1 (2001).
9. B. Janiaud, A. Pumir, D. Bensimon, V. Croquette, H. Richter, L. Kramer, Physica D **55**, 269 (1992).
10. A. Spina, J. Toomre, E. Knobloch, Phys. Rev. E **57**, 524 (1998).
11. P. Kolodner, Phys. Rev. A **46**, 1739 (1992).
12. G.W. Baxter, K.D. Eaton, C.M. Surko, Phys. Rev. A **46**, 1735 (1992).
13. B. Huke, M. Lücke, P. Büchel, Ch. Jung, J. Fluid Mech. **408**, 121 (2000).
14. P. Büchel, M. Lücke, Entropie **218**, 22 (1999).
15. J.K. Platten, J.C. Legros, *Convection in Liquids* (Springer-Verlag, Berlin, Heidelberg, 1984).
16. J.D. Crawford, E. Knobloch, Annu. Rev. Fluid Mech. **23**, 341 (1991).
17. J. Prat, J.M. Massaguer, I. Mercader, Phys. Fluids **7**, 121 (1995).
18. C.K. Mamun, L. Tuckerman, Phys. Fluids **7**, 80 (1995).
19. A. Bergeon, D. Henry, H. BenHadid, L. Tuckerman, J. Fluid Mech. **375**, 143 (1998).
20. V. Frayssé, L. Giraud, S. Gratton, J. Langou, Technical Report TR/PA/03/3, CERFACS (2003). Public domain software available at `www.cerfacs/algor/Softs`.
21. A. Drissi, M. Net, I. Mercader, Phys. Rev. E **60**, 1781 (1999).
22. J. Prat, I. Mercader, E. Knobloch, Phys. Rev. E **58**, 3145 (1998).
23. S. Hugues, A. Randriamampianina, Int. J. Numer. Methods Fluids, **28**, 501 (1998).
24. O. Batiste, M. Net, I. Mercader, E. Knobloch, Phys. Rev. Lett. **86**, 2309 (2001).
25. A. Alonso, O. Batiste Theoret. Comput. Fluid Dyn. **18**, 239 (2004).
26. G. Dangelmayr, J. Hettel, E. Knobloch, Nonlinearity **10**, 1093 (1997).